Engineering NKG2D ligand affinity transforms EGFR-targeted NK cell engagers into high-potency effectors against pancreatic cancer

Seul-Gi Lee[a,†], Myungjee Lee[a,†], Hye-Min Lee[b], Ga-Hyun Son[a], Sang-Rok Yoon[a], Byeong-Ho Chae[a], Dae-Seong Kim[a], Kyung-Mi Lee[b], and Yong-Sung Kim[a,c,*]

[†] These authors contributed equally to this work

[a] Department of Molecular Science and Technology, Ajou University, Suwon 16499, Republic of Korea
[b] Department of Biochemistry and Molecular Biology, College of Medicine, Korea University, Seoul 02841, Republic of Korea
[c] College of Advanced Bio-convergence Engineering, Ajou University, Suwon 16499, Republic of Korea

*To whom correspondence should be addressed: Yong-Sung Kim, Ph.D.
Department of Molecular Science and Technology, Ajou University
206 Worldcup-ro, Yeongtong-gu, Suwon 16499, Korea
Tel.: +82-31-219-2662; E-mail: kimys@ajou.ac.kr
ORCID: Yong-Sung Kim: 0000-0003-2673-1509

This supplementary data includes:
Supplementary Tables 1 to 2
Supplementary Figures 1 to 6

Supplementary Information

Supplementary Table 1. Biochemical and biophysical properties of αEGFR×NKG2DL.

Molecule	MW (kDa)	Purification Yield (mg L^{-1}) [a]	apparent K_D for NKG2D [b]	Target	k_{on} ($M^{-1}s^{-1}$) [c]	k_{off} (s^{-1}) [c]	K_D (nM) [c]	R^2 [c]
αEGFR×dummy	98.4	20.2 ± 1.3	-	EGFR	(4.04 ± 0.21)×10^5	(2.19 ± 0.18)×10^{-4}	0.54 ± 0.05	0.99
αEGFR×MICA	131.1	19.8 ± 1.3	11.6 ± 0.9	EGFR	(5.07 ± 0.18)×10^5	(1.84 ± 0.15)×10^{-4}	0.36 ± 0.03	0.99
				NKG2D	(2.39 ± 0.12)×10^4	(5.49 ± 0.09)×10^{-3}	229 ± 12.4	0.98
αEGFR×MICB	131.1	20.6 ± 1.1	99.1 ± 14.4	EGFR	(3.61 ± 0.18)×10^5	(1.67 ± 0.16)×10^{-4}	0.47 ± 0.05	0.99
				NKG2D	N.Q. [d]	N.Q. [d]	N.Q. [d]	-
αEGFR×ULBP1	120.8	21.4 ± 2.7	119.2 ± 23.1	EGFR	(5.12 ± 0.22)×10^5	(2.18 ± 0.19)×10^{-4}	0.42 ± 0.04	0.99
				NKG2D	N.Q. [d]	N.Q. [d]	N.Q. [d]	-
αEGFR×ULBP2	120.2	19.0 ± 2.4	95.0 ± 17.1	EGFR	(4.24 ± 0.16)×10^5	(1.66 ± 0.13)×10^{-4}	0.39 ± 0.03	0.99
				NKG2D	N.Q. [d]	N.Q. [d]	N.Q. [d]	-
αEGFR×ULBP0601	119.8	17.2 ± 2.6	14.9 ± 0.6	EGFR	(5.52 ± 0.26)×10^5	(3.13 ± 0.22)×10^{-4}	0.57 ± 0.05	0.99
				NKG2D	N.Q. [d]	N.Q. [d]	N.Q. [d]	-
αEGFR×ULBP0602	119.7	22.5 ± 1.7	2.4±0.2	EGFR	(5.81 ± 0.38)×10^5	(3.58 ± 0.33)×10^{-4}	0.62 ± 0.07	0.99
				NKG2D	(2.50 ± 0.06)×10^4	(7.03 ± 0.13)×10^{-4}	28.1 ± 0.82	0.99

[a] Purification yield was calculated from a 100 mL scale HEK293F culture and extrapolated to a 1 L scale. Data are represented as mean ± SD (n = 2).

[b] Apparent K_D was determined by native ELISA using soluble hNKG2D. Data are represented as mean ± SD (n = 3).

[c] Each value represents the mean ± SD of two independent experiments. In each experiment, at least four datasets were used to determine kinetic constants. The association rate constant (k_{on}), dissociation rate constant (k_{off}), equilibrium dissociation constant (K_D), and goodness of fit (R^2) were calculated using Octet Data Analysis software (version 11.0 ForteBio).

[d] N.Q. indicates “not quantifiable”, although experiments were performed.

Supplementary Table 2. Biochemical and biophysical properties of affinity-matured ULBP6-fused αEGFR×ULBP6 ICEs.

Molecule	MW (kDa)	Purification Yield (mg L^{-1}) [a]	k_{on} ($M^{-1}s^{-1}$) [b]	k_{off} (s^{-1}) [b]	K_D (nM) [b]	R^2 [b]	Affinity improvement (fold) [c]
αEGFR×ULBP0602	119.9	27.7 ± 4.0	$(2.77 \pm 0.06)\times10^{4}$	$(8.59 \pm 0.12)\times10^{-4}$	31.0 ± 0.77	0.99	-
αEGFR×ULBP6#1	119.9	28.0 ± 3.6	$(2.07 \pm 0.05)\times10^{4}$	$(7.62 \pm 0.76)\times10^{-5}$	3.67 ± 0.38	0.99	8.4
αEGFR×ULBP6#2	119.9	26.6 ± 3.7	$(3.99 \pm 0.05)\times10^{4}$	$(9.71 \pm 0.64)\times10^{-5}$	2.43 ± 0.16	0.99	12.8
αEGFR×ULBP6#3	120.0	29.2 ± 4.4	$(3.26 \pm 0.08)\times10^{4}$	$(1.36 \pm 0.10)\times10^{-4}$	4.17 ± 0.34	0.99	7.4
αEGFR×ULBP6#4	120.0	29.5 ± 5.4	$(3.19 \pm 0.08)\times10^{4}$	$(2.06 \pm 0.12)\times10^{-4}$	6.44 ± 0.41	0.99	4.8

[a] Purification yield was calculated from a 100 mL scale HEK293F culture and extrapolated to a 1 L scale. Data are represented as mean ± SD (n = 2).

[b] Each value represents the mean ± SD of two independent experiments. In each experiment, at least four datasets were used to determine kinetic constants. The association rate constant (k_{on}), dissociation rate constant (k_{off}), equilibrium dissociation constant (K_D), and goodness of fit (R^2) were calculated using Octet Data Analysis software (version 11.0 ForteBio).

[c] Affinity improvement values indicate the fold increase in NKG2D binding affinity, calculated relative to the K_D of the αEGFR×ULBP0602 ICE.

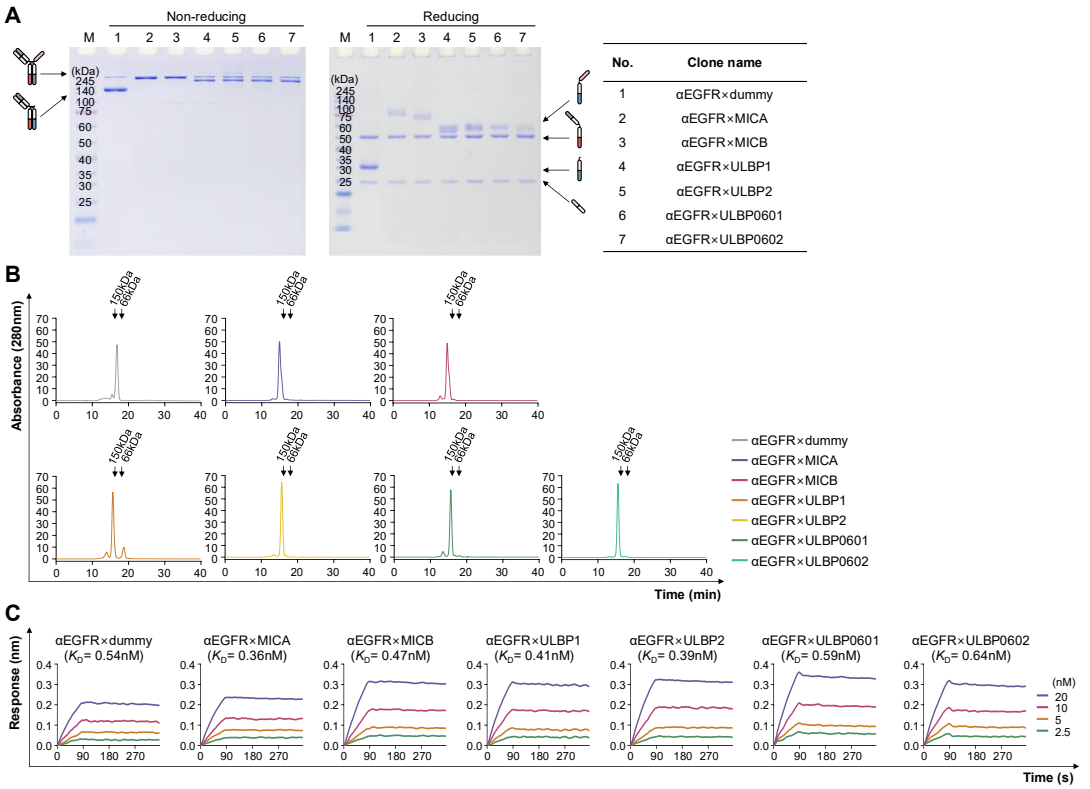

Supplementary Figure 1. Biophysical characterization and EGFR-binding kinetics of αEGFR×NKG2DL ICEs.

(A) SDS-PAGE of purified αEGFR×NKG2DL ICEs (4 μg per lane) under non-reducing and reducing conditions on 12% polyacrylamide gels.

(B) Analytical SEC profiles of αEGFR×NKG2DL ICEs (30 μg per injection) on a Superdex 200 Increase 10/300 column with UV detection at 280 nm. Arrows indicate elution positions of molecular-mass standards (150 kDa, trastuzumab; 66 kDa, bovine serum albumin).

(C) Kinetic analysis of EGFR binding by BLI. Representative sensorgrams are shown with increasing antigen concentrations indicated by color; kinetic parameters (k_{on} and k_{off}) and K_D values are provided in Supplementary Table 1.

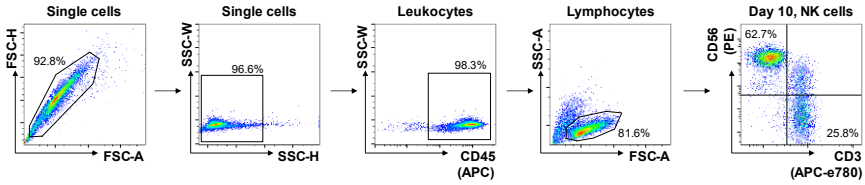

Supplementary Figure 2. Flow-cytometry gating strategy for quantifying NK cells after *ex vivo* expansion of PBMCs.

Representative gating scheme used to identify NK cells in PBMC cultures expanded with KL-1 and EBV-LCL feeder cells in the presence of rhIL-2. NK cells were defined as $CD45^{+}CD3^{-}CD56^{+}$ cells stained with APC conjugated anti-CD45, APC-eFluor 780 conjugated anti-CD3, and PE conjugated anti-CD56. Unstained and isotype controls were included.

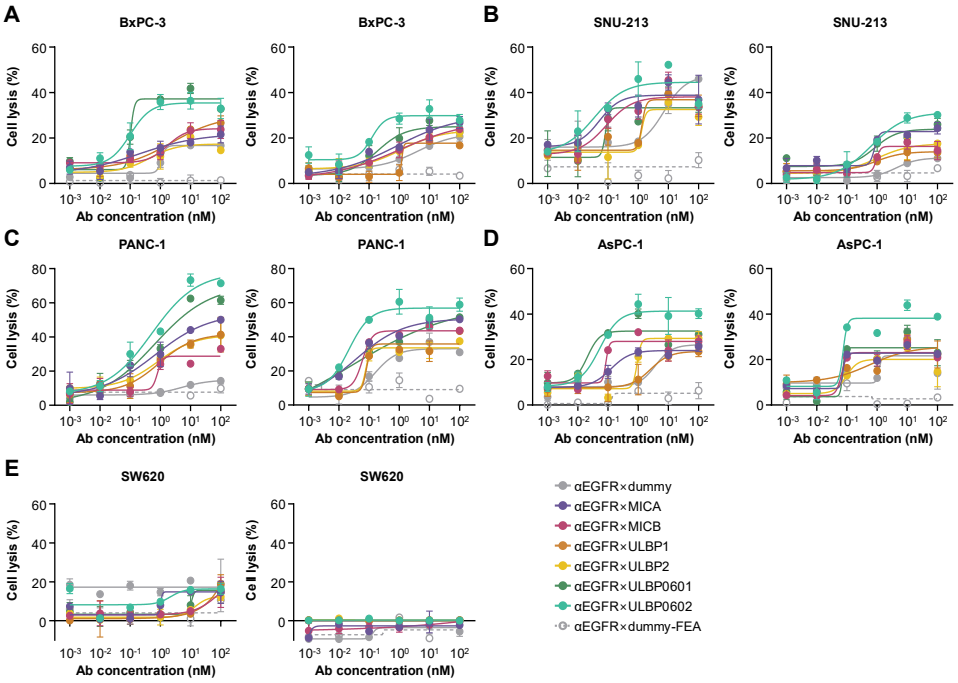

Supplementary Figure 3. ***In vitro*** **cytotoxicity of αEGFR×NKG2DL ICEs using NK cells from additional donors.**

NK cell-mediated cytotoxicity assays were performed as in Fig. 2B using NK cells from two additional donors. Data are shown as mean ± SEM of technical duplicates.

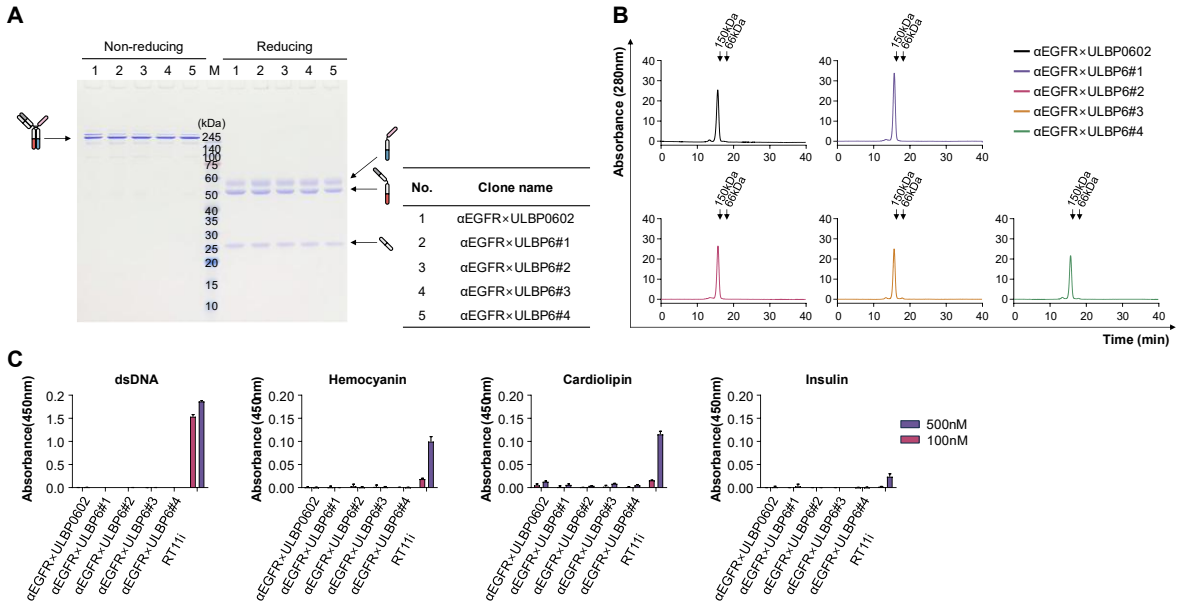

Supplementary Figure 4. Biophysical characterization and nonspecific binding assessment of engineered αEGFR×ULBP6 ICEs.

(A) SDS-PAGE of purified engineered αEGFR×ULBP6 ICEs (4 μg per lane) under non-reducing and reducing conditions on 12% polyacrylamide gels.

(B) Analytical SEC profiles of engineered αEGFR×ULBP6 ICEs (30 μg per injection) on a Superdex 200 Increase 10/300 column monitored at 280 nm. Molecular-mass standards are indicated (150 kDa, trastuzumab; 66 kDa, bovine serum albumin).

(C) Polyspecific binding to immobilized dsDNA, cardiolipin, hemocyanin, and insulin assessed by ELISA; RT11i was used as a positive control. Data are mean ± SD (n = 3).

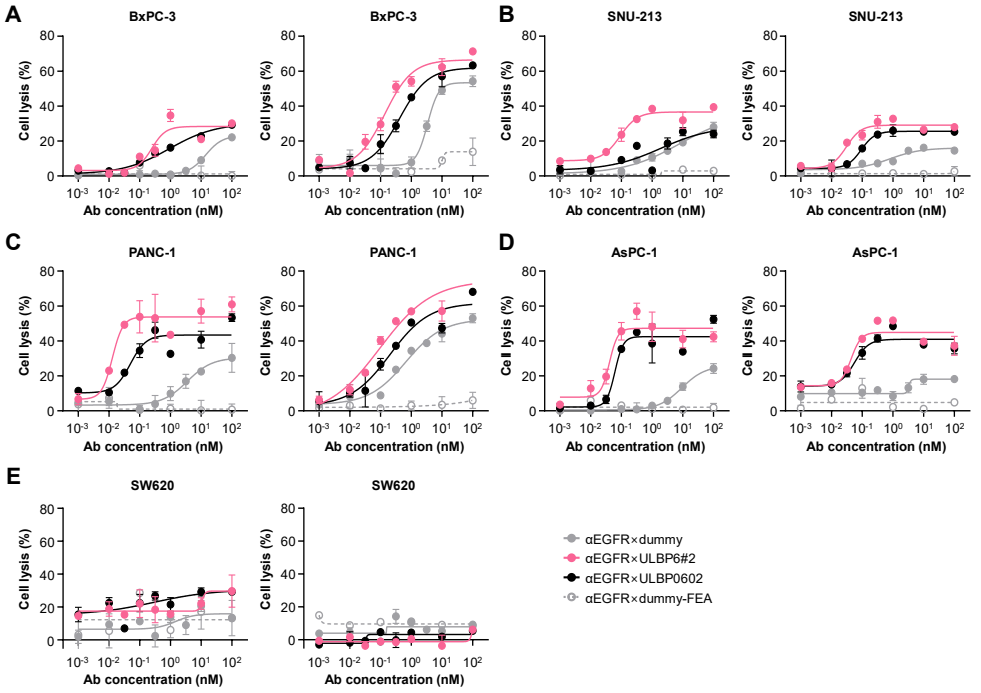

Supplementary Figure 5. *In vitro* cytotoxicity of αEGFR×ULBP6#2 versus αEGFR×ULBP0602 using NK cells from additional donors.

NK cell-mediated cytotoxicity assays were performed as in Fig. 4A and 4B using NK cells from two additional donors. Data are shown as mean ± SEM of technical duplicates.

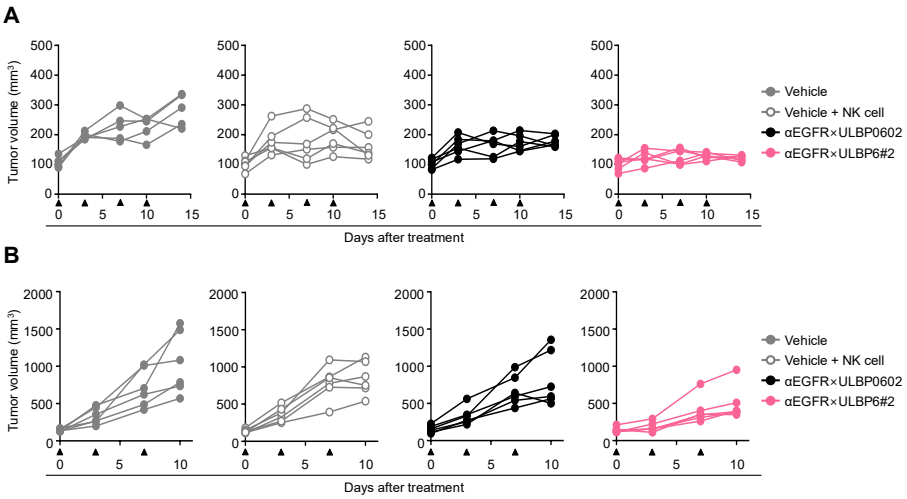

Supplementary Figure 6. Individual tumor growth curves for NK-humanized PDAC xenograft studies.

(A) Individual tumor growth profiles for the PANC-1 group corresponding to Fig. 5B.

(B) Individual tumor growth profiles for the BxPC-3 group corresponding to Fig. 5E.